somal breakpoint occurring outside the c-*mos*–containing sequences encompassed by the 5′-side Bam HI site (5.0 kb upstream of the c-*mos* coding sequence) and the 3′ Bgl II site (5.2 kb downstream of the c-*mos* coding sequence).

Our results indicate that the c-*mos* gene remains on the 8q− chromosome after the t(8;21) in AML. Analysis of complex translocations involving three chromosomes (8, 21, and a third chromosome) has demonstrated that the junction on the 8q− created by the movement of material from chromosome 21 is conserved, whereas the chromosome that donates material to 21 is variable (*16, 17*). The observation that there is a conserved junction in the three-way translocation variants in the t(8;21) of AML, in the t(15;17) in acute promyelocytic leukemia, and in the t(9;22) in chronic myeloid leukemia suggests that the genes or DNA sequences that are relevant to the development of these neoplasias are located in such conserved junctions (*17*). In each of the t(9;22) complex variants that have been analyzed, the c-*abl* gene is translocated to the conserved junction on the 22q− chromosome (*18*). The function of the c-*abl* gene is clearly altered in CML, resulting in transcripts of an abnormal size (*19*) and in protein products of abnormal size and function (*20*).

The association of the c-*mos* gene with the conserved junction of the t(8;21) may be fortuitous, but it is compatible with the hypothesis that this gene is involved in the oncogenic process for this type of leukemia. The finding that no rearrangement of c-*mos* was found in the Southern blot analysis does not exclude this hypothesis, because in other translocations, the breakpoints may be far from the affected genes. For example, in the t(9;22), the breakpoint on chromosome 9 is located from 14 kb to more than 100 kb upstream of the c-*abl* gene (*21*). Moreover, the Daudi line of Burkitt lymphoma cells, which has a t(8;14), has an activated c-*myc* gene, although no rearrangement has been detected within a 25-kb Bam HI fragment (*22*).

Note added in proof: After completion of this manuscript we learned that transcription of c-*mos* was detected in mouse testis, ovary, and embryos (*24*).

References and Notes

1. M. Oskarsson, W. L. McClements, D. G. Blair, J. V. Maizel, G. F. Vande Woude, *Science* **207**, 1222 (1980); D. G. Blair *et al.*, *ibid.* **212**, 941 (1981).
2. G. Rechavi, D. Givol, E. Canaani, *Nature (London)* **300**, 607 (1982); E. Cannani *et al.*, *Proc. Natl. Acad. Sci. U.S.A.* **80**, 7118 (1983).
3. J. B. Cohen, T. Unger, G. Rechavi, E. Canaani, D. Givol, *Nature (London)* **306**, 797 (1983).
4. S. Gattoni-Celli, W. W. Hsiao, I. B. Weinstein, *ibid.*, p. 256.
5. D. J. Slamon, J. B. deKernion, I. M. Verma, M. J. Cline, *Science* **224**, 256 (1984).
6. R. Muller, D. J. Slamon, J. M. Tremblay, M. J. Cline, I. M. Verma, *Nature (London)* **299**, 640 (1982).
7. G. F. Vande Woude, M. Oskarsson, L. W. Enquist, S. Nomura, M. Sullivan, P. J. Fischinger, *Proc. Natl. Acad. Sci. U.S.A.* **76**, 4464 (1979).
8. R. Watson, M. Oskarsson, G. F. Vande Woude, *ibid.* **79**, 4078 (1982).
9. K. Prakash *et al.*, *ibid.*, p. 5210.
10. B. G. Neel, S. C. Jhanwar, R. S. K. Chaganti, W. S. Hayward, *ibid.*, p. 7842.
11. J. Erikson, A. Ar-Rushdi, H. L. Drwinga, P. C. Nowell, C. M. Croce, *ibid.* **80**, 820 (1983); R. Taub *et al.*, *Cell* **36**, 339 (1984).
12. J. D. Rowley, *Ann. Genet.* **16**, 109 (1973).
13. M. Sakurai, M. Oshimura, S. Kakati, A. A. Sandberg, *Lancet* **1974-II**, 227 (1974).
14. H. A. Drabkin *et al.*, *Proc. Natl. Acad. Sci. U.S.A.* **82**, 464 (1985).
15. C. M. Croce *et al.*, *ibid.* **81**, 3170 (1984).
16. V. Lindgren and J. D. Rowley, *Nature (London)* **266**, 744 (1977).
17. J. D. Rowley, *Science* **216**, 749 (1982).
18. C. R. Bartram *et al.*, *Nature (London)* **306**, 277 (1983); A. de Klein and A. Hagemeijer, *Cancer Surveys*, in press.
19. E. Canaani *et al.*, *Lancet* **1984-I**, 593 (1984); R. P. Gale and E. Canaani, *Proc. Natl. Acad. Sci. U.S.A.* **81**, 5648 (1984); S. J. Collins, I. Kubonishi, I. Miyoshi, M. T. Groudine, *Science* **225**, 72 (1984).
20. J. B. Konopka, S. M. Watanabe, O. N. Witte, *Cell* **37**, 1035 (1984).
21. N. Heisterkamp *et al.*, *Nature (London)* **306**, 239 (1983); J. Groffen *et al.*, *Cell* **36**, 93 (1984).
22. R. Dalla-Favera *et al.*, *Proc. Natl. Acad. Sci. U.S.A.* **79**, 7824 (1982).
23. M. M. Le Beau, C. A. Westbrook, M. O. Diaz, J. D. Rowley, *Nature (London)* **312**, 70 (1984).
24. F. Propst and G. F. Vande Woude, *Nature (London)* **315**, 516 (1985).

25. Supported by grants 85-7 of the American Cancer Society and The Leukemia Research Foundation Inc. (M.O.D.), Department of Energy contract DE-AC02-80EV10360, National Institutes of Health grants CA 16910 and CA 25568 (J.D.R.), the University of Chicago Cancer Research Foundation (J.D.R. and M.O.D.), grants HD 13432 from the National Institute for Child Health and AG 00029 from the National Institute of Aging (D.P.), a fellowship from the Leukemia Society of America (M.M.L.) and a fellowship from the Damon Runyon–Walter Winchell Cancer Fund (H.A.D.). The c-*mos*–containing probes were kindly provided by M. Oskarsson and G. Vande Woude; the c-*myc*–containing probe was provided by C. Croce. We acknowledge the technical assistance of A. Harden and R. Espinosa, III.

24 April 1985; accepted 11 June 1985

Noninvasive Study of High-Energy Phosphate Metabolism in Human Heart by Depth-Resolved ^{31}P NMR Spectroscopy

Abstract. *Phosphorus-31 nuclear magnetic resonance (NMR) spectra showing the relative concentrations of high-energy phosphate metabolites have been recorded noninvasively from the human heart in vivo. Spectral data were spatially localized by combining a pulsed magnetic field gradient with surface NMR excitation-detection coils. The location of the selected spectral region was determined by conventional proton NMR imaging immediately before examination by phosphorus-31 NMR spectroscopy.*

PAUL A. BOTTOMLEY
General Electric Corporate Research and Development Center, Schenectady, New York 12301

Current noninvasive clinical techniques for assessing injury in heart disease utilize the anatomical information provided by x-ray computed tomography, ultrasound imaging, γ cameras, emission tomography, and proton (^{1}H) nuclear magnetic resonance (NMR) imaging techniques. Limited information on relative perfusion and glucose and fatty acid metabolism in the heart is also available from γ cameras and emission tomography by administration of isotopically labeled pharmaceuticals (*1*). An advantage of metabolic probes in general is that physiologic changes affecting heart function are virtually immediately detectable and can precede anatomic changes by days or more. Such probes are therefore better suited to monitoring therapeutic response.

Recent applications of natural-abundance phosphorus-31 (^{31}P) NMR to the detection of high-energy phosphate metabolism in vivo have provided valuable diagnostic information about various muscular and cerebral disorders in adults and infants without the use of ionizing radiation (*2*). ^{31}P NMR studies of isolated perfused rodent hearts have revealed transient metabolic response to drug therapies (*3, 4*), cardiotoxic chemotherapeutic agents (*5*), and global and regional ischemia (*6*) in times as short as 1.5 minutes after onset (*7*). In most cases, pathology is detected by ^{31}P NMR spectroscopy as disturbances in the ratios of the high-energy metabolites phosphocreatine (PCr) and adenosine triphosphate (ATP) as well as inorganic phosphate (P_i).

The in vivo ^{31}P heart studies have been extended in situ by enclosing the heart in an NMR coil either permanently implanted or in open-chest animals (*8–10*); by using catheter NMR coils inserted through a peripheral blood vessel (*11*); and by restricting the NMR spectrometer sensitivity to the heart by magnetic field profiling and using an external NMR coil with the surface musculature of the subject surgically removed (*12*). This work was limited to rodents and dogs, and the techniques were rendered invasive by the necessity of ensuring adequate spatial localization of the ^{31}P

NMR signal. We have developed an alternative, noninvasive technique (called depth-resolved surface coil spectroscopy, DRESS) for recording localized ^{31}P NMR spectra in vivo (*13*). This technique has now permitted observation of ^{31}P NMR spectra showing phosphorus metabolism in the human heart.

Spectra were recorded by means of a small, circular, tuned, flat NMR coil located outside the chest and adjacent to the heart. The coil was used for both transmission and detection of the NMR signal from a selected slice parallel to the plane of the coil. Slice selection was accomplished with a sinc function–modulated, radio-frequency (RF) excitation pulse applied in the presence of a magnetic field gradient directed coaxial to the coil. The amplitude of the RF pulse was adjusted to maximize the detected signal. First, the amplitude was calibrated for maximum signal for a slice close to the surface of the subject's chest. The amplitude at other slice depths was then calculated from known curves for the spatial dependence of the magnetic field along the coil axis (*14*). The extent of the signal contributions from the selected slice was confined approximately to a disk in the plane of the slice by the sensitivity profile of the surface coil (*13*). The precise location of the coil and of the excited sensitive disk relative to the heart was determined by conventional ^{1}H NMR imaging (*15*). Imaging with a whole-body NMR coil and with a ^{1}H NMR surface coil of the same size as the ^{31}P NMR coil provided coarse and fine positioning information, respectively (*16*). The depth of the slice was adjusted either by moving the subject relative to the slice or, automatically, by offsetting the NMR frequency in a single side-band transmitter.

Figure 1 demonstrates application of the technique to the liver of a normal volunteer using a 1.5-T, 1-m bore NMR imaging–spectroscopy research system (*13, 15*). Unlike chest and abdominal wall muscle, liver contains negligible PCr (*17*). It therefore serves as a useful test in vivo of the ability of spatial localization techniques to discriminate between NMR signal contributions from surface and deep tissue. A 6.5-cm ^{1}H NMR coil was positioned above the right costal margin, and conventional coronal (depth, 5 cm) and sagittal images were recorded (slice thickness, 0.5 cm) at 62 MHz, depicting the slice location in the liver (Fig. 1, A and B). Integration of the image intensity (*16*) in Fig. 1A indicated

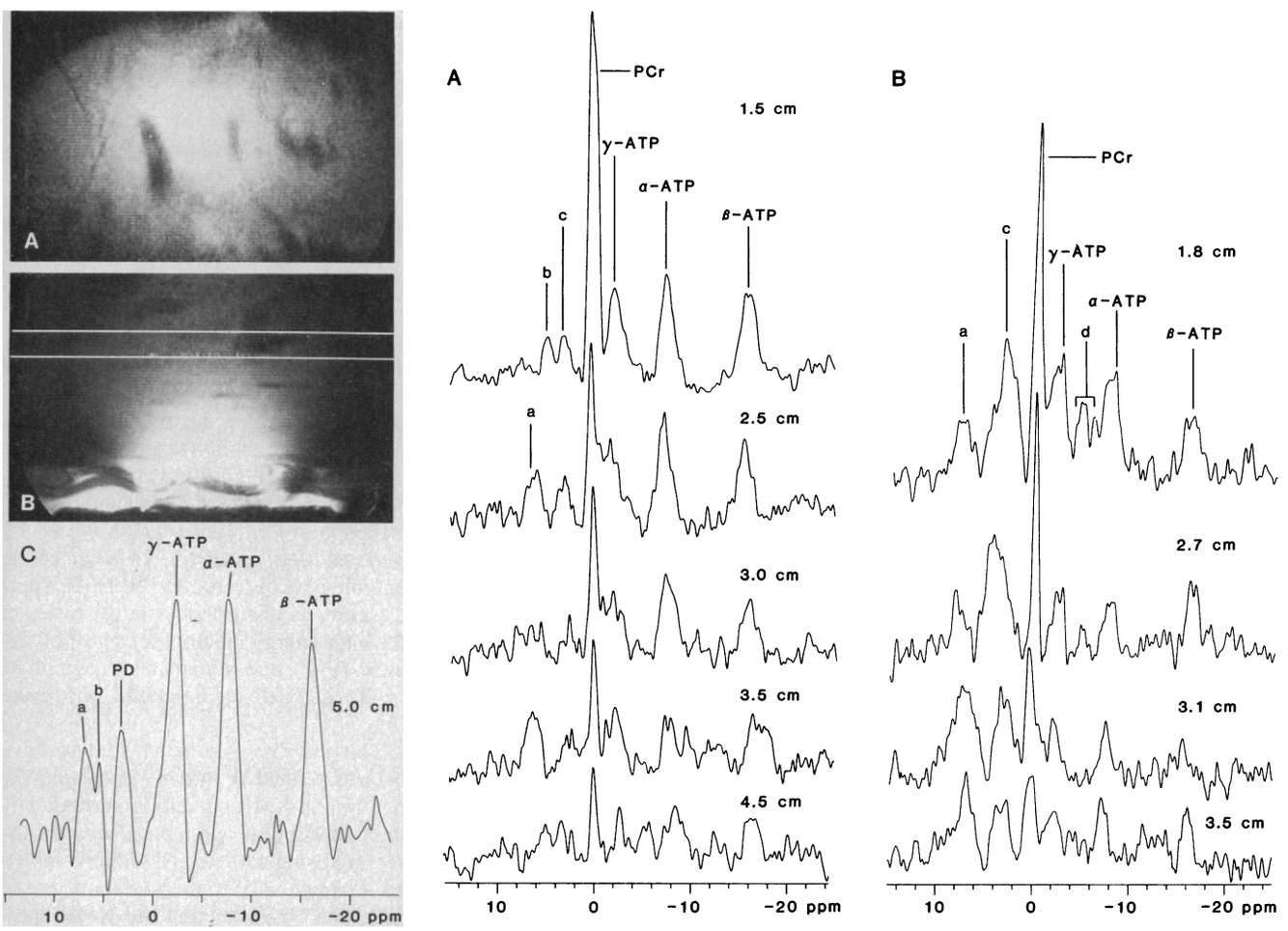

Fig. 1 (left). Conventional coronal (A) and sagittal (B) ^{1}H NMR images (slice thickness, 0.5 cm) of human liver recorded in vivo by means of a 6.5-cm surface coil for both transmission and reception. (A) The ^{1}H NMR signal distribution in a plane at a depth of 5 cm delineated relative to the surface in (B) (array size, 256 by 256 points; scan time, 4 minutes). The ^{31}P NMR spectrum (C) was recorded from a slice (thickness, 1.2 cm) in the same location as that imaged in (A) with a 6.5-cm ^{31}P surface coil (1200 acquisitions; 1-second repetition period; 8-Hz exponential filter). α-, β-, and γ-ATP are the α-, β-, and γ-phosphates of ATP [γ- and α-ATP resonances include contributions from other nucleoside phosphates (*2-12*)]; PD is the phospodiester resonance. Chemical shifts are relative to PCr at 0.0 ppm. Fig. 2 (right). ^{31}P NMR spectra recorded as a function of depth with the 6.5-cm surface coil over the left ventricle (A) (600 acquisitions; 1-second repetition period; 8-Hz exponential filter) and displaced 5 cm to the right over the right ventricle (B) (1200 acquisitions; 1-second repetition period; same filter). Spectrometer gains for each series are constant except for the 1.5-cm spectrum, which is halved. Depths are nominally relative to the surface with the subject prone on top of the surface soil.

that 50 percent of the total ^1H NMR signal from the selected plane derived from a sensitive disk 7 cm in diameter. A ^1H NMR spectrum was also recorded from the entire coronal slice by switching off all imaging gradients except for the slice selection gradient; this spectrum was used to optimize the magnetic field homogeneity by adjusting the currents in external magnetic field gradient shim coils (*3, 13*). The spectrum contained a single H_2O resonance with a negligible mobile lipid ($-CH_2-$) peak, indicative of a healthy liver without fat deposits (*18*). Typical line widths of the H_2O resonance from selected slices in the body were 0.1 to 0.3 part per million (ppm). The ^1H coil was then immediately replaced by a 6.5-cm ^{31}P coil at exactly the same location, and a ^{31}P NMR spectrum was recorded from the slice at 25.1 MHz with the same gradient. For constant gradient strength and RF pulse duration, the slice thickness increased from 0.5 cm to 1.2 cm in the ^{31}P experiment; that is, by the ratio of the NMR frequencies of ^1H to ^{31}P (*13*). The absence of PCr in the spectrum (Fig. 1C) is consistent with its liver source. Switching between ^1H and ^{31}P operation required only resetting of the NMR spectrometer frequency and connecting the ^{31}P coil and coil-tuning network to the NMR spectrometer.

Series of spectra recorded as a function of depth by means of the above procedure but with the ^{31}P coil positioned on the chest over the septum and left ventricle and over the right ventricle of the subject's heart are shown in Fig. 2, A and B. ^1H NMR images corresponding to Fig. 2B were obtained with a whole-body imaging coil and denote the location of the surface coil by intensity artifacts in Fig. 3, which arose from the mutual interactions of the coils. Body and surface-coil images were also recorded for the geometry represented by Fig. 2A. Spectra were recorded with a 1-second pulse repetition period, but the ratio of the PCr to ATP resonances was substantially unchanged at 3.5 cm depth when the repetition period was extended to 8 seconds. Thus NMR pulse-flip angles were less than $\pi/2$ at the selected planes, and heart spectra were undistorted by spin-lattice relaxation effects (*16*). Neither the image nor the spectral acquisition was synchronized with the cardiac or respiratory cycles, so that motion artifacts were removed by signal averaging. Thus the data predominantly correspond to the diastolic phase of the heart. Some variations in high-energy phosphate metabolites have been observed within the cardiac cycle in isolated perfused hearts (*19*), but not in situ (*10*). The decrease in coil sensitivity as a function of depth prohibited acquisition of satisfactory 20-minute spectra from depths of 5 cm or greater.

Two striking features of the spectra in Fig. 2 are the large decrease in the ratio of PCr to ATP between shallow and deep slices and the changes in peak amplitude in the 5 to 8 ppm region (peak a). The former feature was due to a transition from predominantly skeletal chest muscle to predominantly heart muscle. The ratio of PCr to β-ATP (mean ± standard deviation) was 1.3 ± 0.4 as calculated by integrating the area under these resonances in spectra from the septum and left ventricle at depths of 2.5, 3, 3.5, and 4.5 cm and from the right ventricle at depths of 3.1 and 3.5 cm. This value is consistent with values obtained from the invasive studies of animals in situ [1.7 ± 0.2 (*8*), 1.33 ± 0.15 (*10*), and 1.7 estimated from Fig. 4 (*11*)]. Peak a has been assigned to 2,3-diphosphoglycerate (DPG) in blood (*8, 9, 11, 12*) and to phosphomonoesters in general (*10, 11*). The former assignment could explain variations in the amplitude of this peak among heart spectra as a reflection of differing proportions of blood in different slices. The two DPG phosphate resonances in blood occur around 6 ppm and are separated by less than 1 ppm (*11*). They are unresolved here and elsewhere (*11*), possibly because of blood flow effects. Contributions to PCr and ATP peaks from blood are negligible (*8, 11*). Peaks b and c can be assigned to P_i and phosphodiesters. Peak d is unassigned.

The diameter of the sensitive disk enclosing 50 percent of the signal was about 6 cm at a depth of 3 cm and about 5 cm at a depth of 2 cm. In addition to blood, lung tissue and pericardial fat could also have contributed to the deep spectra. However, lung tissue has a low density and is therefore unlikely to contribute substantially, and the ^1H NMR spectra used for optimizing the magnetic field homogeneity in slices at depths greater than 3 cm exhibited a mobile $-CH_2-$ resonance about 20 times weaker than the H_2O resonance. This suggests that the contribution to the spectra from fat was minimal; fat is low in high-energy metabolites anyway. We therefore conclude that the PCr and ATP resonances in the deep spectra derived almost entirely from the heart muscle.

Initial experiments on dogs have indicated that regional ischemia is detectable noninvasively in the heart by ^{31}P NMR with the technique described here (*20*). Also, the DRESS method can be extended to yield multiple spectra from different depths in the same time as is required to obtain a single spectrum by successively exciting different slices within the normal pulse repetition period (*21*). The ability to obtain metabolically useful information from the heart by ^{31}P NMR in reasonable scan times renders clinical applications quite practical.

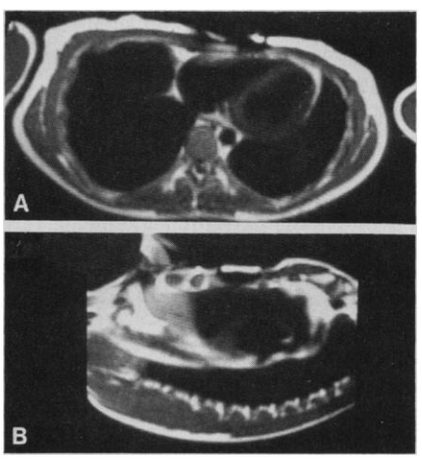

Fig. 3. Axial (A) and sagittal (B) ^1H NMR images through the heart and lung fields recorded with a whole-body imaging coil (array size, 256 by 256 points; slice thickness, 0.5 cm; scan time, 4 minutes). The images depict the relative location of the surface coil used for acquiring spectra in Fig. 2B as intensity artifacts (dark structure, top center) above the right ventricle of the heart. Images (A) and (B) are oriented chest-upward; image (A) looks toward the head, and the abdomen is to the left-hand side of image (B). The subject was prone on top of the surface coil. The spectra in Fig. 2A were recorded with the surface coil displaced 5 cm to the right on image (A). Coronal images recorded from the body coil and from a ^1H NMR surface coil at a depth of 3.1 cm corresponding to Fig. 2B showed the heart muscle surrounded by pericardial fat and heart muscle, respectively.

References and Notes

1. G. L. Brownell *et al.*, *Science* **215**, 619 (1982).
2. R. D. Ross *et al.*, *N. Engl. J. Med.* **304**, 1338 (1981); R. J. Newman *et al.*, *Brit. Med. J.* **284**, 1072 (1982); G. K. Radda *et al.*, *Nature (London)* **295**, 608 (1982); R. H. T. Edwards *et al.*, *Lancet* **1982-I**, 725 (1982); E. B. Cady *et al.*, *ibid.* **1983-I**, 1059 (1983); D. L. Arnold *et al.*, *ibid.* **1984-I**, 1367 (1984); P. L. Hope *et al.*, *ibid.* **1984-II**, 366 (1984).
3. R. L. Nunnally and P. A. Bottomley, *Science* **211**, 177 (1981).
4. P. M. Mathews *et al.*, *Biochim. Biophys. Acta* **720**, 163 (1982); M. Nakazawa *et al.*, *J. Cadiovasc. Pharmacol.* **4**, 700 (1982); R. J. Newman and G. K. Radda, *Brit. J. Pharmacol.* **79**, 395 (1983); J. P. Dhasmana *et al.*, *J. Cardiovasc. Pharmacol.* **5**, 1040 (1983).
5. T. C. Ng *et al.*, *Biochem. Biophys. Res. Commun.* **110**, 339 (1983).
6. W. E. Jacobus *et al.*, *Nature (London)* **265**, 756 (1977); P. M. Mathews *et al.*, *Biochim. Biophys. Acta* **721**, 312 (1982); A. C. Pernot *et al.*, *Circulation* **67**, 1296 (1983).
7. D. P. Hollis *et al.*, *J. Magn. Reson.* **29**, 319 (1978).
8. T. H. Grove *et al.*, *Proc. Natl. Acad. Sci. U.S.A.* **77**, 299 (1980).
9. K. J. Neurohr *et al.*, *FEBS Lett.* **159**, 207 (1984).

10. A. P. Koretsky *et al.*, *Proc. Natl. Acad. Sci. U.S.A.* **80**, 7491 (1983).
11. H. L. Kantor, R. W. Briggs, R. S. Balaban, *Circ. Res.* **55**, 261 (1984).
12. H. Tamatsu *et al.*, *Jpn. J. Pharmacol.* **34**, 375 (1984).
13. P. A. Bottomley, T. H. Foster, R. D. Darrow, *J. Magn. Reson.* **59**, 338 (1984).
14. A. Haase *et al.*, *ibid.* **55**, 164 (1983).
15. P. A. Bottomley *et al.*, *Radiology* **150**, 441 (1984).
16. P. A. Bottomley *et al.*, *Magn. Reson. Med.* **1**, 410 (1984).
17. R. E. Gordon *et al.*, *Nature (London)* **287**, 736 (1980); R. A. Iles and J. R. Griffiths, *Biosci. Rep.* **2**, 735 (1982).
18. J. K. T. Lee *et al.*, *Radiology* **153**, 195 (1984).
19. E. T. Fossel, H. E. Morgan, J. S. Ingwall, *Proc. Natl. Acad. Sci. U.S.A.* **77**, 3654 (1980).
20. P. A. Bottomley *et al.*, in preparation.
21. P. A. Bottomley *et al.*, *J. Magn. Reson.*, in press.
22. I thank J. Piel, C. J. Hardy, L. S. Smith, and O. M. Mueller for technical assistance, and R. W. Redington, J. F. Schenck, and S. Brazzamano for useful discussions.

4 March 1985; accepted 12 June 1985

Ethanol Withdrawal in Mice Precipitated and Exacerbated by Hyperbaric Exposure

Abstract. *Mice were fed an ethanol-containing liquid diet for 9 days. On removal of the diet, exposure to 12 atmospheres absolute of a mixture of helium and oxygen precipitated earlier withdrawal, increased withdrawal scores for the first 6 hours, and increased the peak withdrawal intensity compared to dependent animals exposed to control conditions. The enhanced withdrawal did not appear to reflect alterations in ethanol elimination, oxygen or helium partial pressures, body temperature, or general excitability. These results extend to chronically treated animals the evidence that hyperbaric exposure antagonizes the membrane actions of ethanol.*

RONALD L. ALKANA
DEBORAH A. FINN
GUNTWIN G. GALLEISKY
Alcohol and Brain Research Laboratory, Institute for Toxicology, School of Pharmacy, University of Southern California Los Angeles 90033
PETER J. SYAPIN
Department of Neurology, School of Medicine, and *Alcohol and Brain Research Laboratory, School of Pharmacy, University of Southern California*
RICHARD D. MALCOLM*
Alcohol and Brain Research Laboratory, Institute for Toxicology, School of Pharmacy, University of Southern California

*Present address: Smith Kline & French Laboratories, P.O. Box 1608, San Anselmo, California 94960.

Current molecular theories of general anesthesia are based on the physicochemical properties of anesthetics rather than on specific receptor interactions (*1–4*). These theories postulate that general anesthetics, including ethanol, act by penetrating hydrophobic lipid or protein regions in brain cell plasma membranes. The resultant perturbations are thought to lead to conformational changes in membrane-bound proteins, altering their function and thereby causing cellular depression and anesthesia. The exact site of anesthetic action is unknown, but evidence suggests that perturbations in discrete microenvironments in the membrane are more likely to be the critical events than are changes in the bulk membrane (*3, 4*). Perturbation theories are supported, in part, by the ability of increased hydrostatic and atmospheric pressure to reverse or reduce the acute depressant effects of ethanol and other general anesthetics (*2, 3, 5*). It is hypothesized that the increased pressure blocks or counteracts anesthetic-induced perturbations, thereby returning the membrane components to their original conformational and functional states.

Chronic exposure to ethanol can lead to the development of tolerance and physical dependence (*6*). These phenomena, including the hyperexcitability and convulsions seen after ethanol is removed from dependent animals, are thought to reflect compensatory changes that offset the acute effects of ethanol (*7*). If increased atmospheric pressure antagonizes the acute effects of ethanol by blocking or counteracting its action on membranes, then exposure to hyperbaric environments should precipitate or enhance withdrawal in ethanol-dependent animals. The augmented withdrawal would be analogous to the effect of opiate antagonists on morphine-dependent animals (*8*).

In previous studies we observed that exposure to 12 atmospheres absolute (ATA) of a mixture of helium and oxygen antagonizes the acute depressant effect of ethanol in mice (*5, 9–12*). The antagonism does not reflect changes in the absorption, distribution, or elimination of ethanol; increases in the partial pressure of oxygen or helium; or alterations in body temperature. In the present study we found that exposure to 12 ATA of helium + oxygen precipitates and exacerbates withdrawal in ethanol-dependent mice. To our knowledge, this is the first evidence that hyperbaric exposure behaves as an ethanol antagonist in chronically treated animals.

Drug-naïve adult male C57BL/6J mice were made physically dependent on ethanol by exposure for 9 days to a liquid ethanol-containing diet (F711A; Bio-Serv, Inc.) as the sole source of water and nutrients (*13*). The animals were housed individually in a room kept at 21° ± 1°C with a 12-hour light-dark cycle (lights on at 0700 hours). Diet consumption and intoxication scores (*14*) were recorded daily before fresh diet was supplied at 0800 hours.

The withdrawal period was initiated at 0200 hours on day 9 by removing the diet. The mice were moved to new individual housing consisting of clear plexiglass tubes (8 by 20.5 cm) and were randomly assigned to one of the following conditions: 1 ATA of air at 25°C; 1 ATA of helium + oxygen at 30°C; or 12 ATA of helium + oxygen at 30°C (*15*). We used a higher chamber temperature in the helium + oxygen conditions to offset the cooling effect of helium and thereby eliminate the potential for confounded results due to differences in body temperature (*10, 14, 16*). Three 18-liter chambers, holding up to seven mice each, were used to test the three treatment conditions simultaneously (*17*). The atmospheric gas content, pressure, and flow rate were adjusted with compressed air or helium + oxygen. The procedures ensured adequate oxygenation during and after compression and set the final partial pressure of oxygen at 0.2 ATA (*5, 12*). Withdrawal signs (*14*) were rated hourly for 14 hours by an observer who was unaware of the chamber conditions. The hourly score for each mouse was based on its behavior during a 2-minute observation period at the beginning of each hour. There were no statistically significant differences in withdrawal scores between the group exposed to 1 ATA of helium + oxygen and the group exposed to 1 ATA of air (Fig. 1 and Table 1). Therefore, the data for these two groups were pooled for statistical comparisons with the 12 ATA group.

Hyperbaric exposure precipitated and intensified the signs of ethanol withdrawal (Fig. 1 and Table 1). The mice in the 12 ATA group exhibited signs of withdrawal at the first rating period 1 hour after the ethanol diet was removed. In contrast, the 1 ATA air group did not show any signs of withdrawal until the second hourly rating (Fig. 1). The mean withdrawal scores for the 12 ATA group were 23 to 134 percent greater than those for